Science Advances
AAAS

advances.sciencemag.org/cgi/content/full/7/17/eabd9275/DC1

Supplementary Materials for

Ultrafast dynamical Lifshitz transition

Samuel Beaulieu*, Shuo Dong, Nicolas Tancogne-Dejean*, Maciej Dendzik, Tommaso Pincelli, Julian Maklar, R. Patrick Xian, Michael A. Sentef, Martin Wolf, Angel Rubio, Laurenz Rettig, Ralph Ernstorfer*

*Corresponding author. Email: samuel.beaulieu@u-bordeaux.fr (S.B.); nicolas.tancogne-dejean@mpsd.mpg.de (N.T.-D.); ernstorfer@fhi-berlin.mpg.de (R.E.)

Published 21 April 2021, *Sci. Adv.* **7**, eabd9275 (2021)
DOI: 10.1126/sciadv.abd9275

This PDF file includes:

I. Additional experimental data

Dynamics along X-Γ-X

In Fig. 2 of the main paper, we presented differential Fermi surfaces and cuts along Y-Γ-Y ($k_x = 0$) direction, to show the unambiguous signature of Lifshitz transition. Our multidimensional detection scheme allows us to measure differential signals along any direction of the Brillouin zone with sufficient counting statistics. To compare our data with previously published time- and angle-resolved photoemission spectroscopy (ARPES) results on the same material, we can plot the photoemission differential signal along X-Γ-X ($k_y = 0$) high-symmetry direction, as reported by Crepaldi *et al.* [38]. The strong enhancement of the signal around $\pm$ 0.25 $Å^{-1}$ above the Fermi level, the depletion around Γ below the Fermi level, as well as the extracted excited states lifetime of $\sim$ 270 fs, from our experimental data presented on Fig. S1, is in good agreement with the observations of Crepaldi *et al.*, who studied the enhanced ultrafast relaxation rate in the Weyl semimetallic (low temperature) phase of $MoTe_2$. In that paper, the authors didn't report the dynamics along Γ-Y, which is the direction along which the signature of the Lifshitz transition is the most evident.

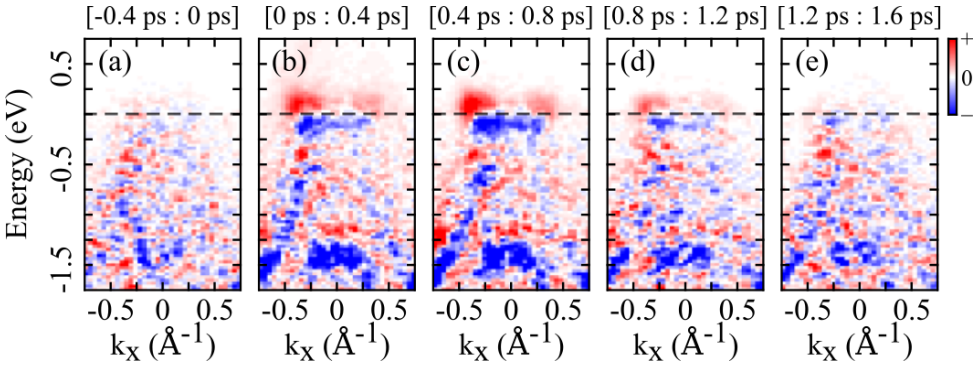

Figure S1: **Ultrafast electronic dynamic along X-Γ-X.** (a)-(e) Differential (signal before time-zero subtracted) energy-resolved cuts along X-Γ-X ($k_y = 0$) as a function of time delay between the IR pump and the XUV probe. These data are extracted from the same scan as for Fig. 2 of the main text. The pump pulse intensity is estimated to be 6.7x10^9 W/cm^2.

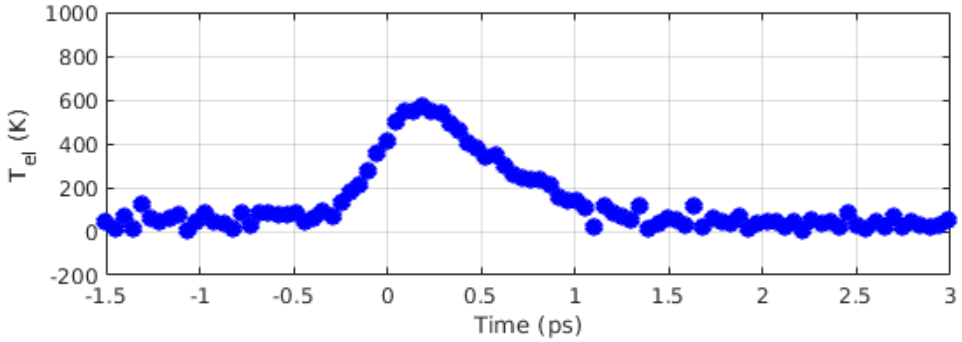

Figure S2: **Time-dependent electronic temperature.**: Electronic temperature as a function of pump-probe delay, extracted from fitting the energy distribution-curve (integrated along Γ-X) by a resolution-broadened Fermi-Dirac distribution function.

Time-dependent electronic temperature

We have extracted the time-dependent electronic temperature, to estimate the heating of the electronic system by the pump pulse. This information provides a reference point for theoretical simulations, presented in the next sections. To do so, we fitted the energy distribution-curve (EDCs) (integrated along Γ-X) measured experimentally by Fermi-Dirac distribution functions convoluted with a Gaussian function as the spectral instrument response function. We have used EDCs obtained by integrating the signal along Γ-X, in order to exclude the effect of the time-dependent density of states along Γ-Y, which could introduce some ambiguity in the fitting procedure.

First, we have fixed the electronic temperature of the Fermi-Dirac distribution to 30 K and kept the Gaussian width as a free parameter of the fit, for the case of the unpumped system, to estimate the instrument response function. Next, we have fixed the instrument response function (the Gaussian width), and fit a Fermi-Dirac distribution for each pump-probe delay, keeping the electronic temperature as a free parameter of the fit. The results of the fit are shown in Fig. S2.

As shown in Fig. S2, after the interaction with the pump laser pulse, the electronic temperature increases to almost 600 K and then gradually recovers to the original temperature of

$\sim$ 30 K, within a time-scale similar to the excited states population lifetime (signal above the Fermi level). As explained in the theoretical section of the Supplementary Information, this increase of the electronic temperature (dynamical populations), combined with the dynamical modification of Hubbard U_{eff}, is at the origin of the ultrafast non-equilibrium Lifshitz transition.

Fitting the γ-pocket position

In order to extract the position of the bottom of the γ-pocket for different pump-probe delays, we have fitted the energy distribution curves, taken at the Y point of the Brillouin zone. We have fitted two Gaussian separated by 36.5 meV (upper and lower bands at Y) weighted by the instrument response function broaden time-dependent Fermi-Dirac distribution extracted from the fit of the EDC along Γ-X (region where the band structure is not modified upon photoexcitation). Examples of such EDCs fitting are shown in Fig. S3.

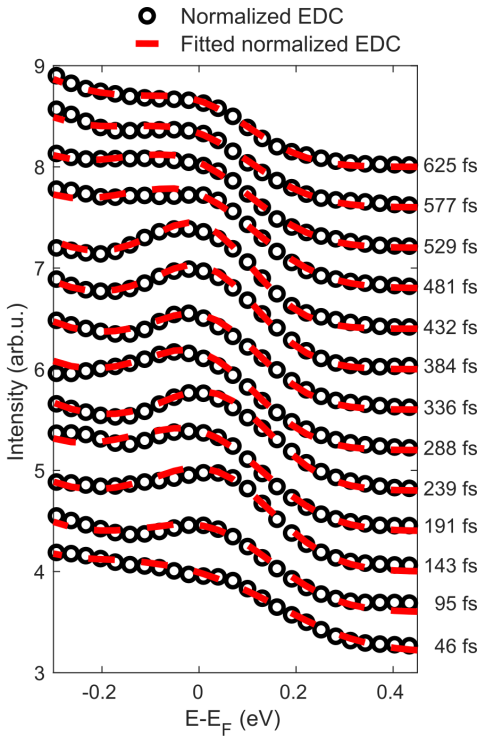

Figure S3: **Energy distribution curves fitting**: The black dots are normalized experimentally measured EDC cuts at the Y point of the Brillouin zone, for different pump-probe delays (indicated on the right side of the figure). The dashed red lines are the results of the EDC fitting.

II. Adiabatic Lifshitz transition

We first theoretically analyze the adiabatic Lifshitz transition and in particular the effect of U_{eff} on the energy position of the γ-pocket. For this, we performed a set of DFT+U calculations while varying U_{eff}. Our results are shown in Fig. 1c in the main text. The self-consistently evaluated U_{eff} is found to be 2.05 eV. From our calculations, we find that the Lifshitz transition occurs around 1.5 eV, which is consistent with the value obtained from a similar analysis by Xu *et al.* [15].

From these data, we find that in the adiabatic limit, for a 70 meV change in position of the γ-pocket, which has been measured experimentally, (see Fig. 3c in the main text), a change in U_{eff} of 1.8 eV is required. This is in clear contrast with the results obtained in Fig. 3e from our

TDDFT+U calculations, from which the change in U_{eff} at the experimental intensity is estimated to be around 30 meV only. Thus, our results indicate that the measured energy downshifts of the pocket, ultimately leading to the Lifshitz transition, cannot originate only from an adiabatic change of U_{eff} and that more subtle dynamics are at play here.

Note that we carefully checked that the laser-induced changes in U_{eff} are converged and that adding more $\mathbf{k}$-point to sample the Brillouin zone do not lead to sizable differences in the dynamics of U_{eff}. Moreover, note that due to numerical artifacts, the Fig. 3a and Fig. 3b are obtained without spin-orbit coupling included. Whereas the main results are not affected by the inclusion or not of the spin-orbit coupling, the Wannierization procedure, employed to get the Fermi surface cut from the non-equilibrium states, is found to be less stable when the spin-orbit coupling is included.

We want to point out the analogy to the creation of a Weyl semimetallic phase induced by a laser in pyrochlore iridates, that some of us predicted [19]. Indeed, in this previous work, we showed that light-induced reduction of U_{eff} is leading to the transient appearance of a Weyl semimetallic phase in pyrochlore irridate for values of U_{eff} for which, according to the equilibrium (adiabatic) phase diagram, should not allow it.

The experimentally measured change in the pocket position also shows a clear delay between the change in the pocket energy position and the laser pulse itself (timed by the LAPE signal, Fig. 3b in the main text), indicating that some transient dynamics still takes place after the end of the laser pulse and before the material starts to returns to its ground state due to thermalization effects. This is an indication that the system is brought to a non-equilibrium state at the end of the laser pulse.

As discussed below, our results provide evidence explaining the observed light-induced Lifshitz transition, but we found that one needs to take into account the non-equilibrium dynamics induced by the laser and not only a simpler adiabatic change of the Hubbard U_{eff}.

III. Non-equilibrium Fermi surface

From the theoretical point of view, the Fermi surface is a concept that is well defined at equilibrium, and for a vanishing temperature. However, in time- and angle-resolved photoemission experiments, it is possible to measure the Fermi surface evolving in time for a fixed Fermi energy, taking as reference the equilibrium value. Here, we aim at comparing this measured non-equilibrium Fermi surface to the results of our time-dependent simulations, which include both the change in populations and time-evolved Hubbard U. We employed for this the non-equilibrium states taken after the end of the laser pulse and computed the corresponding energies

$$E^{\mathrm{neq}}_{n\mathbf{k}}(t) = \langle \psi_{n\mathbf{k}}(t) | \hat{H}(t) | \psi_{n\mathbf{k}}(t) \rangle, \tag{1}$$

where n refers to a band index, $\mathbf{k}$ is the $\mathbf{k}$-point index, $\psi_{n\mathbf{k}}(t)$ the Pauli spinor representing the Bloch state obtained from the time-evolution of the TDDFT Kohn-Sham equations, and $\hat{H}[n(t)](t)$ is the Hamiltonian constructed from the time-evolved electronic density $n(t)$ as well as $U_{\mathrm{eff}}(t)$ and the corresponding non-equilibrium occupations $n^{\sigma\sigma'}_{mm'}(t)$.

We note that using these energies after the end of the laser pulse (*i.e.* when there is no vector potential due to the laser) makes the result of our analysis gauge invariant. Alternatively, one might want to use the adiabatic eigenvalues, $E^{ad}_{n\mathbf{k}}(t)$, of the time-evolved Hamiltonian, $\hat{H}(t)$, to investigate the non-equilibrium Fermi surface defined by

$$\hat{H}(t) | \psi^{\mathrm{ad}}_{n\mathbf{k}} \rangle = E^{\mathrm{ad}}_{n\mathbf{k}}(t) | \psi^{\mathrm{ad}}_{n\mathbf{k}} \rangle. \tag{2}$$

Here, similar to the previous case, $\hat{H}(t)$ is the Hamiltonian constructed from the time-evolved electronic density $n(t)$ as well as $U_{\mathrm{eff}}(t)$ and the corresponding non-equilibrium occupations $n^{\sigma\sigma'}_{mm'}(t)$.

We found that the adiabatic states do not show any Lifshitz transition compared to the non-equilibrium states, which is fully consistent with our analysis above. Indeed, if the adiabatic

states would show a Lifshitz transition, the band structure corresponding to the Hamiltonian constructed from $U(t)$ would show a Lifshitz transition, which we have shown not to be the case for the excitation density used in this experiment. This is a strong indication of the non-adiabatic nature of the measured Lifshitz transition.

IV. Effect of dynamical U

We further analyze the role of the different ingredients to reach the Lifshitz transition. From the theoretical results presented in the main text, the change of U_{eff} is found to be quite small in Fig. 3e, compared to what could be expected from the equilibrium phase diagram (Fig. 1c in the main text), in order to reach the Lifshitz transition. To disentangle the different effects taking place, we also performed a time-dependent simulation with a frozen U_{eff} and compared with the result with a time-evolving U_{eff} presented in the main text. This analysis allows us to clearly identify the role of dynamical U_{eff} in driving the Lifshitz transition. Indeed, for a time-dependent U_{eff}-frozen simulation, the non-adiabatic nature of the time-evolved states is still taken into account, as well as dynamical populations, as described by the local-density approximation, but the dynamical correlations (captured by time-evolving U_{eff}) are not included.

For a clearer comparison with the experimental results, we simulate a differential angle-resolved photoemission signal from the excited-state eigenvalues. We employed Wannier90 [39] to interpolate the band structures on a finer k-point grid. We, then, convoluted in energy and in momentum by a Gaussian whose widths correspond to the experimental resolutions, respectively 120 meV and 0.05Å^{-1}.

Our results are shown in Fig. S4 for the Y-Γ-Y direction, *i.e.* the direction where the hallmark of the Lifshitz transition, and we found that γ-pocket crossing the Fermi level, appears. From these data, it is clear that the appearance of the γ-pocket in the angle-resolved photoemission signal crucially depends on the dynamical U_{eff}. Indeed, in Fig. S4(b), the signal of the

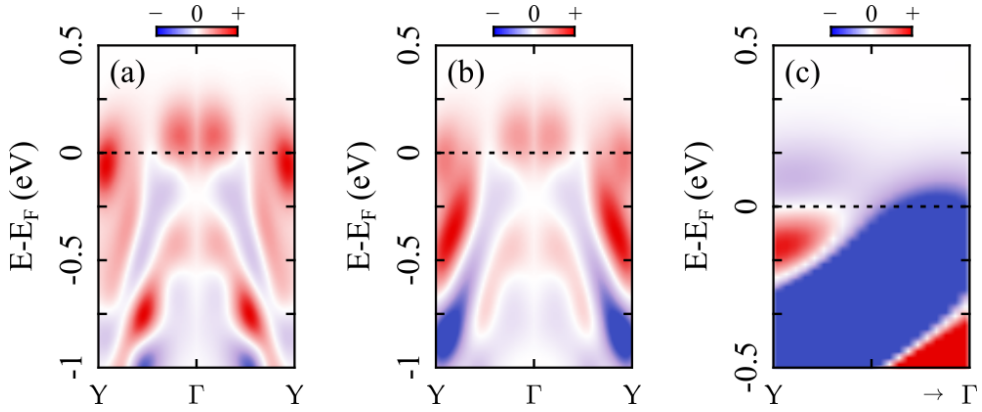

Figure S4: **Effect of dynamical U_{eff} along Y-Γ-Y.** a) Calculation performed from the excited states obtained at the end of the laser pulse for a dynamical U_{eff} calculation. b) Same as a) but for a frozen U_{eff} calculation. The (a) and (b) panels correspond to simulated differential maps, similar to what is measured experimentally. c) Difference of the two signals, *i.e.* (a) and (b), close to the position of the pocket.

pocket does not appear clearly, whereas it is the dominating feature in Fig. S4(a). As evidenced by the difference close to the position of the γ-pocket, which displays a clear differential profile, the dynamical U_{eff} calculation yields a pocket below the Fermi energy whereas the frozen U_{eff} approach yields a pocket at higher energy. In other words, as shown in Fig. S4(c), the dynamical U_{eff} case leads to such a down-shift compared to the frozen U calculation, and the differential profile is occurring at the Fermi energy. This clearly shows that the dynamical U_{eff} leads to a down-shift of the pocket below the Fermi energy, whereas the frozen U_{eff} does not. Otherwise, the differential profile would be centered around a value below the Fermi energy.

This is a clear indication that the dynamical correlations are a crucial ingredient to observe the Lifshitz transition.

We also computed similar plots for the X-Γ-X direction (see Fig. S5) for which U_{eff} is expected not to play an important role. As expected, we do not observe any qualitative difference between the frozen and dynamical U_{eff} calculations, confirming the validity of our approach.

Importantly, in both cases, we note that the simulated ARPES spectra are qualitative agree-

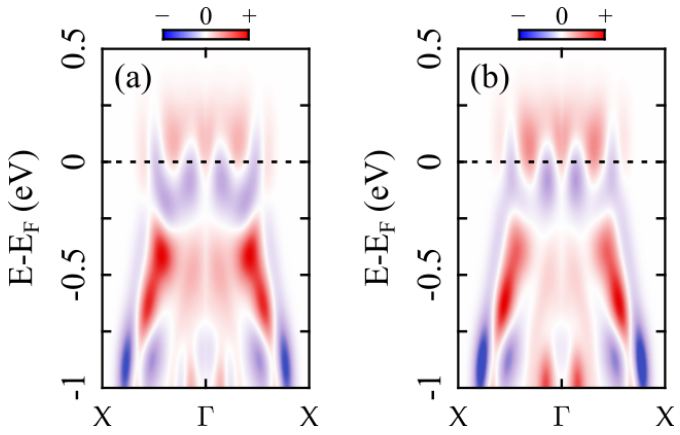

Figure S5: **Effect of dynamical U_{eff} along X-Γ-X.** a) Calculation performed from the excited states obtained at the end of the laser pulse for a dynamical U_{eff} calculation. b) Same as a) but for a frozen U_{eff} calculation. These panels correspond to simulated differential maps, similar to what is measured experimentally.

ment with the experimental ARPES signals (see Fig. 2 in the main text and Fig. S1). Finally, we note that these results employ here a crude approximation to the measured ARPES signal, in which transition dipole matrix elements are not taken into account, which would correspond to more intricate and numerically more expensive TDDFT calculations in supercell [40].

V. Note on the role of dynamical populations

As shown in the main text, the full TDDFT+U_{eff} simulations, which include both the dynamical evolution of U_{eff} and of the populations, predict the ultrafast Lifshitz transition. Moreover, the comparison between the non-equilibrium simulations performed with frozen and with dynamical U_{eff} (Fig. S4) showed that even if Hubbard U_{eff} do not reach the adiabatic critical value ($U_{\text{eff}} \sim 1.5$ eV) to reach the Lifshitz transition, the inclusion of dynamical U_{eff} is essential to reach the non-equilibrium Lifshitz transition. By taking into account these observations, we argue that both the dynamical modification of the U_{eff}, and of the populations, are necessary to reach the ultrafast non-equilibrium Lifshitz transition. This also implies that the novel non-equilibrium route requires a significantly smaller change in the Hubbard U_{eff} than the adiabatic

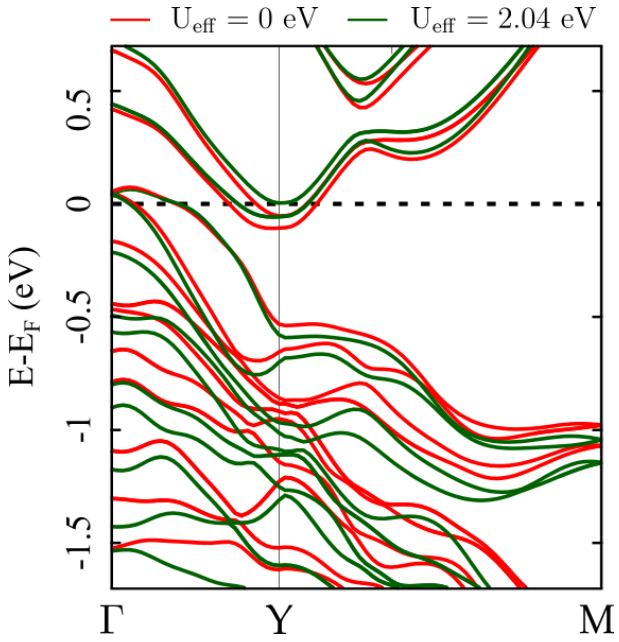

Figure S6: **Band structure of** $1\mathrm{T}'$**-**$\mathrm{MoTe_2}$. The electronic band structure of $1\mathrm{T}'$-$\mathrm{MoTe_2}$ for the equilibrium self-consistent value of U_{eff} = 2.04 eV (in green) and for the reduced value of U_{eff} = 0 eV.

case to reach the Lifshitz transition.

VI. Band structure of $1\mathrm{T}'$-$\mathrm{MoTe_2}$

We also performed simulations for the $1\mathrm{T}'$-phase of $\mathrm{MoTe_2}$ (see Fig. S6), which is the high temperature phase. We employed the same parameters as for equilibrium studies of $\mathrm{T_d}$-$\mathrm{MoTe_2}$, and used the previously reported atomic coordinates [33]. We performed both DFT and DFT+U calculations, in which we evaluated the *ab initio* U_{eff}, see Sec. III for more details. As an important result, we found that even including a Hubbard U_{eff} of 2.04 eV (obtained from first principles), the γ-pocket of the $1\mathrm{T}'$ phase of $\mathrm{MoTe_2}$ is located below the Fermi energy.

This shows that at equilibrium, the $1\mathrm{T}'$- and the $\mathrm{T_d}$-phase have different Fermi surface topologies. This raises the question of whether the measured data corresponds to a light-induced structural phase transition to the high-temperature $1\mathrm{T}'$ phase, as observed in Ref. [28]. We argue

in detail in the main text that this is not the case. Briefly, the pump fluence that we used ($\sim$ 0.6 mJ/cm^2) is significantly lower than the structural phase transition critical fluence ($>$2 mJ/cm^2), and the time-scales relevant for the experimentally observed Lifshitz transition are completely different than the ones associated with the light-induced structural phase transition [28].

REFERENCES AND NOTES

1. M. I. Kaganov, I. M. Lifshitz, Electron theory of metals and geometry. *Physics-Uspekhi* **22**, 904-927 (1979).
2. Y. Wu, N. H. Jo, M. Ochi, L. Huang, D. Mou, S. L. Bud'ko, P. C. Canfield, N. Trivedi, R. Arita, A. Kaminski, Temperature-induced Lifshitz transition in WTe_2. *Phys. Rev. Lett.* **115**, 166602 (2015).
3. Y. Zhang, C. Wang, L. Yu, G. Liu, A. Liang, J. Huang, S. Nie, X. Sun, Y. Zhang, B. Shen, J. Liu, H. Weng, L. Zhao, G. Chen, X. Jia, C. Hu, Y. Ding, W. Zhao, Q. Gao, C. Li, S. He, L. Zhao, F. Zhang, S. Zhang, F. Yang, Z. Wang, Q. Peng, X. Dai, Z. Fang, Z. Xu, C. Chen, X. J. Zhou, Electronic evidence of temperature-induced Lifshitz transition and topological nature in $ZrTe_5$. *Nat. Commun.* **8**, 15512 (2017).
4. F. C. Chen, Y. Fei, S. J. Li, Q. Wang, X. Luo, J. Yan, W. J. Lu, P. Tong, W. H. Song, X. B. Zhu, L. Zhang, H. B. Zhou, F. W. Zheng, P. Zhang, A. L. Lichtenstein, M. I. Katsnelson, Y. Yin, N. Hao, Y. P. Sun, Temperature-induced Lifshitz transition and possible excitonic instability in ZrSiSe. *Phys. Rev. Lett.* **124**, 236601 (2020).
5. Z. J. Xiang, G. J. Ye, C. Shang, B. Lei, N. Z. Wang, K. S. Yang, D. Y. Liu, F. B. Meng, X. G. Luo, L. J. Zou, Z. Sun, Y. Zhang, X. H. Chen, Pressure-induced electronic transition in black phosphorus. *Phys. Rev. Lett.* **115**, 186403 (2015).
6. D. Kang, Y. Zhou, W. Yi, C. Yang, J. Guo, Y. Shi, S. Zhang, Z. Wang, C. Zhang, S. Jiang, A. Li, K. Yang, Q. Wu, G. Zhang, L. Sun, Z. Zhao, Superconductivity emerging from a suppressed large magnetoresistant state in tungsten ditelluride. *Nat. Commun.* **6**, 7804 (2015).
7. V. Sunko, E. Abarca Morales, I. Markovic, M. E. Barber, D. Milosavljevic, F. Mazzola, D. A. Sokolov, N. Kikugawa, C. Cacho, P. Dudin, H. Rosner, C. W. Hicks, P. D. C. King, A. P. Mackenzie, Direct observation of a uniaxial stress-driven Lifshitz transition in Sr_2RuO_4. *npj Quant. Mater.* **4**, 46 (2019).
8. B. Burganov, C. Adamo, A. Mulder, M. Uchida, P. D. C. King, J. W. Harter, D. E. Shai, A. S. Gibbs, A. P. Mackenzie, R. Uecker, M. Bruetzam, M. R. Beasley, C. J. Fennie, D. G. Schlom, K. M. Shen, Strain control of Fermiology and many-body interactions in two-dimensional ruthenates. *Phys. Rev. Lett.* **116**, 197003 (2016).
9. A. Ptok, K. J. Kapcia, A. Cichy, A. M. Oleś, P. Piekarz, Magnetic Lifshitz transition and its consequences in multi-band iron-based superconductors. *Sci. Rep.* **7**, 41979 (2017).

10. C. Liu, T. Kondo, R. M. Fernandes, A. D. Palczewski, E. D. Mun, N. Ni, A. N. Thaler, A. Bostwick, E. Rotenberg, J. Schmalian, S. L. Bud'ko, P. C. Canfield, A. Kaminski, Evidence for a Lifshitz transition in electron-doped iron arsenic superconductors at the onset of superconductivity. *Nat. Phys.* **6**, 419-423 (2010).
11. X. Shi, Z.-Q. Han, X.-L. Peng, P. Richard, T. Qian, X.-X. Wu, M.-W. Qiu, S. C. Wang, J. P. Hu, Y.-J. Sun, H. Ding, Enhanced superconductivity accompanying a Lifshitz transition in electron-doped FeSe monolayer. *Nat. Commun.* **8**, 14988 (2017).
12. I. M. Lifshitz, Anomalies of electron characteristics of a metal in the high pressure region. *J. Exp. Theor. Phys.* **38**, 1569 (1960).
13. Y. Wang, M. N. Gastiasoro, B. M. Andersen, M. Tomić, H. O. Jeschke, R. Valentí, I. Paul, P. J. Hirschfeld, Effects of Lifshitz transition on charge transport in magnetic phases of Fe-based superconductors. *Phys. Rev. Lett.* **114**, 097003 (2015).
14. H. Chi, C. Zhang, G. Gu, D. E. Kharzeev, X. Dai, Q. Li, Lifshitz transition mediated electronic transport anomaly in bulk $ZrTe_5$. *New J. Phys.* **19**, 015005 (2017).
15. N. Xu, Z. W. Wang, A. Magrez, P. Bugnon, H. Berger, C. E. Matt, V. N. Strocov, N. C. Plumb, M. Radovic, E. Pomjakushina, K. Conder, J. H. Dil, J. Mesot, R. Yu, H. Ding, M. Shi, Evidence of a Coulomb-interaction-induced Lifshitz transition and robust hybrid Weyl semimetal in T_d-$MoTe_2$. *Phys. Rev. Lett.* **121**, 136401 (2018).
16. D. Kutnyakhov, R. P. Xian, M. Dendzik, M. Heber, F. Pressacco, S. Y. Agustsson, L. Wenthaus, H. Meyer, S. Gieschen, G. Mercurio, A. Benz, K. Bühlman, S. Däster, R. Gort, D. Curcio, K. Volckaert, M. Bianchi, C. Sanders, J. A. Miwa, S. Ulstrup, A. Oelsner, C. Tusche, Y.-J. Chen, D. Vasilyev, K. Medjanik, G. Brenner, S. Dziarzhytski, H. Redlin, B. Manschwetus, S. Dong, J. Hauer, L. Rettig, F. Diekmann, K. Rossnagel, J. Demsar, H.-J. Elmers, P. Hofmann, R. Ernstorfer, G. Schönhense, Y. Acremann, W. Wurth, Time- and momentum-resolved photoemission studies using time-of-flight momentum microscopy at a free-electron laser. *Rev. Sci. Instrum.* **91**, 013109 (2020).
17. N. Tancogne-Dejean, M. J. T. Oliveira, A. Rubio, Self-consistent DFT + *U* method for real-space time-dependent density functional theory calculations. *Phys. Rev. B* **96**, 245133 (2017).
18. N. Tancogne-Dejean, M. A. Sentef, A. Rubio, Ultrafast modification of Hubbard *U* in a strongly correlated material: Ab initio high-harmonic generation in NiO. *Phys. Rev. Lett.* **121**, 097402 (2018).

19. G. E. Topp, N. Tancogne-Dejean, A. F. Kemper, A. Rubio, M. A. Sentef, All-optical nonequilibrium pathway to stabilising magnetic Weyl semimetals in pyrochlore iridates. *Nat. Commun.* **9**, 4452 (2018).
20. A. A. Soluyanov, D. Gresch, Z. Wang, Q. Wu, M. Troyer, X. Dai, B. A. Bernevig, Type-II Weyl semimetals. *Nature* **527**, 495-498 (2015).
21. X. Wan, A. M. Turner, A. Vishwanath, S. Y. Savrasov, Topological semimetal and Fermi-arc surface states in the electronic structure of pyrochlore iridates. *Phys. Rev. B* **83**, 205101 (2011).
22. S.-Y. Xu, I. Belopolski, N. Alidoust, M. Neupane, G. Bian, C. Zhang, R. Sankar, G. Chang, Z. Yuan, C.-C. Lee, S.-M. Huang, H. Zheng, J. Ma, D. S. Sanchez, B. Wang, A. Bansil, F. Chou, P. P. Shibayev, H. Lin, S. Jia, M. Z. Hasan, Discovery of a Weyl fermion semimetal and topological Fermi arcs. *Science* **349**, 613–617 (2015).
23. P. Hosur, X. Qi, Recent developments in transport phenomena in Weyl semimetals. *Comptes Rendus Physique* **14**, 857 - 870 (2013).
24. N. Aryal, E. Manousakis, Importance of electron correlations in understanding photoelectron spectroscopy and Weyl character of $MoTe_2$. *Phys. Rev. B* **99**, 035123 (2019).
25. M. Puppin, Y. Deng, C. W. Nicholson, J. Feldl, N. B. M. Schröter, H. Vita, P. S. Kirchmann, C. Monney, L. Rettig, M. Wolf, R. Ernstorfer, Time- and angle-resolved photoemission spectroscopy of solids in the extreme ultraviolet at 500 kHz repetition rate. *Rev. Sci. Instrum.* **90**, 023104 (2019).
26. K. Medjanik, O. Fedchenko, S. Chernov, D. Kutnyakhov, M. Ellguth, A. Oelsner, B. Schönhense, T. R. F. Peixoto, P. Lutz, C.-H. Min, F. Reinert, S. Däster, Y. Acremann, J. Viefhaus, W. Wurth, H. J. Elmers, G. Schönhense, Direct 3D mapping of the Fermi surface and Fermi velocity. *Nat. Mater.* **16**, 615-621 (2017).
27. J. Maklar, S. Dong, S. Beaulieu, T. Pincelli, M. Dendzik, Y. W. Windsor, R. P. Xian, M. Wolf, R. Ernstorfer, L. Rettig, A quantitative comparison of time-of-flight momentum microscopes and hemispherical analyzers for time- and angle-resolved photoemission spectroscopy experiments. *Rev. Sci. Instrum.* **91**, 123112 (2020).
28. M. Y. Zhang, Z. X. Wang, Y. N. Li, L. Y. Shi, D. Wu, T. Lin, S. J. Zhang, Y. Q. Liu, Q. M. Liu, J. Wang, T. Dong, N. L. Wang, Light-induced subpicosecond lattice symmetry switch in $MoTe_2$. *Phys. Rev. X* **9**, 021036 (2019).
29. H. L. Kiwia, E. F. Westrum Jr, Low-temperature heat capacities of molybdenum diselenide and ditelluride. *J. Chem. Thermodyn.* **7**, 683–691 (1975).

30. F. C. Chen, H. Y. Lv, X. Luo, W. J. Lu, Q. L. Pei, G. T. Lin, Y. Y. Han, X. B. Zhu, W. H. Song, Y. P. Sun, Extremely large magnetoresistance in the type-II Weyl semimetal $MoTe_2$. *Phys. Rev. B* **94**, 235154 (2016).
31. M. Yankowitz, S. Chen, H. Polshyn, Y. Zhang, K. Watanabe, T. Taniguchi, D. Graf, A. F. Young, C. R. Dean, Tuning superconductivity in twisted bilayer graphene. *Science* **363**, 1059–1064 (2019).
32. R. P. Xian, Y. Acremann, S. Y. Agustsson, M. Dendzik, K. Buhlmann, D. Curcio, D. Kutnyakhov, F. Pressacco, M. Heber, S. Dong, T. Pincelli, J. Demsar, W. Wurth, P. Hofmann, M. Wolf, M. Scheidgen, L. Rettig, R. Ernstorfer, An open-source, end-to-end workflow for multidimensional photoemission spectroscopy. *Sci. Data* **7**, 442 (2020).
33. Y. Qi, P. G. Naumov, M. N. Ali, C. R. Rajamathi, W. Schnelle, O. Barkalov, M. Hanfland, S.-C. Wu, C. Shekhar, Y. Sun, V. Süß, M. Schmidt, U. Schwarz, E. Pippel, P. Werner, R. Hillebrand, T. Förster, E. Kampert, S. Parkin, R. J. Cava, C. Felser, B. Yan, S. A. Medvedev, Superconductivity in Weyl semimetal candidate $MoTe_2$. *Nat. Commun.* **7**, 11038 (2016).
34. N. Tancogne-Dejean, M. J. T. Oliveira, X. Andrade, H. Appel, C. H. Borca, G. L. Breton, F. Buchholz, A. Castro, S. Corni, A. A. Correa, U. D. Giovannini, A. Delgado, F. G. Eich, J. Flick, G. Gil, A. Gomez, N. Helbig, H. Hübener, R. Jestädt, J. Jornet-Somoza, A. H. Larsen, I. V. Lebedeva, M. Lüders, M. A. L. Marques, S. T. Ohlmann, S. Pipolo, M. Rampp, C. A. Rozzi, D. A. Strubbe, S. A. Sato, C. Schäfer, I. Theophilou, A. Welden, A. Rubio, Octopus, a computational framework for exploring light-driven phenomena and quantum dynamics in extended and finite systems. *J. Chem. Phys.* **152**, 124119 (2020).
35. X. Andrade, D. Strubbe, U. De Giovannini, A. H. Larsen, M. J. T. Oliveira, J. Alberdi-Rodriguez, A. Varas, I. Theophilou, N. Helbig, M. J. Verstraete, L. Stella, F. Nogueira, A. Aspuru-Guzik, A. Castro, M. A. L. Marques, A. Rubio, Real-space grids and the octopus code as tools for the development of new simulation approaches for electronic systems. *Phys. Chem. Chem. Phys.* **17**, 31371-31396 (2015).
36. A. Castro, H. Appel, M. Oliveira, C. A. Rozzi, X. Andrade, F. Lorenzen, M. A. L. Marques, E. K. U. Gross, A. Rubio, Octopus: a tool for the application of time-dependent density functional theory. *Phys. Status Solidi B* **243**, 2465-2488 (2006).
37. L. A. Agapito, S. Curtarolo, M. Buongiorno Nardelli, Reformulation of DFT + *U* as a pseudohybrid hubbard density functional for accelerated materials discovery. *Phys. Rev. X* **5**, 011006 (2015).

38. A. Crepaldi, G. Autès, G. Gatti, S. Roth, A. Sterzi, G. Manzoni, M. Zacchigna, C. Cacho, R. T. Chapman, E. Springate, E. A. Seddon, P. Bugnon, A. Magrez, H. Berger, I. Vobornik, M. Kalläne, A. Quer, K. Rossnagel, F. Parmigiani, O. V. Yazyev, M. Grioni, Enhanced ultrafast relaxation rate in the Weyl semimetal phase of $MoTe_2$ measured by time- and angle-resolved photoelectron spectroscopy. *Phys. Rev. B* **96**, 241408 (2017).
39. G. Pizzi, V. Vitale, R. Arita, S. Blügel, F. Freimuth, G. Géranton, M. Gibertini, D. Gresch, C. Johnson, T. Koretsune, J. Ibañez-Azpiroz, H. Lee, J.-M. Lihm, D. Marchand, A. Marrazzo, Y. Mokrousov, J. I. Mustafa, Y. Nohara, Y. Nomura, L. Paulatto, S. Poncé, T. Ponweiser, J. Qiao, F. Thöle, S. S. Tsirkin, M. Wierzbowska, N. Marzari, D. Vanderbilt, I. Souza, A. A. Mostofi, J. R. Yates, Wannier90 as a community code: New features and applications. *J. Phys. Condens. Matter* **32**, 165902 (2020).
40. U. De Giovannini, H. Hubener, A. Rubio, A first-principles time-dependent density functional theory framework for spin and time-resolved angular-resolved photoelectron spectroscopy in periodic systems. *J. Chem. Theory Comput.* **13**, 265–273 (2016).